Influence of enzyme immobilization and skin-sensor interface on non-invasive glucose determination from interstitial fluid obtained by magnetohydrodynamic extraction

Kemp, Emily

2022-06-15

Kemp , E , Palomaki , T , Ruuth , I A , Boeva , Z A , Nurminen , T A , Vanska , R T , Zschaechner , L K , Perez , A G , Hakala , T A , Wardale , M , Haeggstrom , E & Bobacka , J 2022 , ' Influence of enzyme immobilization and skin-sensor interface on non-invasive glucose determination from interstitial fluid obtained by magnetohydrodynamic extraction ' , Biosensors & Bioelectronics , vol. 206 , 114123 . https://doi.org/10.1016/j.bios.2022.114123

http://hdl.handle.net/10138/343097
https://doi.org/10.1016/j.bios.2022.114123

Biosensors and Bioelectronics 206 (2022) 114123

Contents lists available at ScienceDirect

Biosensors and Bioelectronics

journal homepage: www.elsevier.com/locate/bios

Influence of enzyme immobilization and skin-sensor interface on non-invasive glucose determination from interstitial fluid obtained by magnetohydrodynamic extraction

Emily Kemp [a,1], Tommi Palomäki [a,1], Ida A. Ruuth [a,1], Zhanna A. Boeva [a,b], Teemu A. Nurminen [a], Risto T. Vänskä [a], Laura K. Zschaechner [a], Alejandro García Pérez [a], Tuuli A. Hakala [a], Melissa Wardale [a], Edward Haeggström [a,c], Johan Bobacka [a,b,*]

[a] GlucoModicum Ltd, A.I. Virtasen Aukio 1, 00560, Helsinki, Finland
[b] Laboratory of Molecular Science and Engineering, Faculty of Science and Engineering, Åbo Akademi University, Henriksgatan 2, 20500, Åbo, Finland
[c] Department of Physics, University of Helsinki, Gustaf Hällströmin katu 2, 00560, Helsinki, Finland

ARTICLE INFO

Keywords:
Magnetohydrodynamic extraction
Wearable glucose biosensor
Skin-sensor interface
Electrospun nanofiber
Hydrogel

ABSTRACT

We integrated a magnetohydrodynamic fluid extractor with an amperometric glucose biosensor to develop a wearable device for non-invasive glucose monitoring. Reproducible fluid extraction through the skin and efficient transport of the extracted fluid to the biosensor surface are prerequisites for non-invasive glucose monitoring. We optimized the enzyme immobilization and the interface layer between the sensing device and the skin. The monitoring device was evaluated by extracting fluid through porcine skin followed by glucose detection at the biosensor. The biosensor featured a screen-printed layer of Prussian Blue that was coated with a layer containing glucose oxidase. Both physical entrapment of glucose oxidase in chitosan and tethering of glucose oxidase to electrospun nanofibers were evaluated. Binding of glucose oxidase to nanofibers under mild conditions provided a stable biosensor with analytical performance suitable for accurate detection of micromolar concentrations of glucose. Hydrogels of varying thickness (95–2000 μm) as well as a thin (30 μm) nanofibrous polycaprolactone mat were studied as an interface layer between the biosensor and the skin. The effect of mass transfer phenomena at the biosensor-skin interface on the analytical performance of the biosensor was evaluated. The sensing device detected glucose extracted through porcine skin with an apparent (overall) sensitivity of −0.8 mA/(M·cm^2), compared to a sensitivity of −17 mA/(M·cm^2) for measurement in solution. The amperometric response of the biosensor correlated with the glucose concentration in the fluid that had been extracted through porcine skin with the magnetohydrodynamic technique.

1. Introduction

Recently, we reported (Garcia Perez et al., 2019; Hakala et al., 2021) that when a magnetic field is applied locally and in combination with an electric field, it induces a Lorentz force that transports interstitial fluid to the skin surface. The phenomenon is called magnetohydrodynamic (**MHD**) extraction. Similarly to reverse iontophoresis (Bandodkar et al., 2015; Kurnik et al., 1998; Lipani et al., 2018; Pikal, 2001; Rao et al., 1995, 1993; Sieg et al., 2004; Tierney et al., 1999), MHD extraction can be used to extract interstitial fluid for diagnostic purposes. MHD extraction has several advantages over reverse iontophoresis, e.g., low applied electric current and short extraction times. These factors potentially improve the representativeness of the interstitial fluid sample and speed up the analysis.

We chose glucose as an analyte to demonstrate the relevance of MHD extraction for diagnostic purposes. Diabetes management has societal and economic significance and glucose monitoring devices provide a way to control blood sugar levels in diabetic patients. However, these devices often require skin puncture to access capillary blood (Blum, 2018). The MHD technology does neither pierce nor disrupt the skin layers and, following several reviews on the topic (Bandodkar and Wang, 2014; Kim et al., 2018; Wang, 2008), we considered a wearable

* Corresponding author. GlucoModicum Ltd, A.I. Virtasen Aukio 1, 00560, Helsinki, Finland.
E-mail address: johan.bobacka@abo.fi (J. Bobacka).
[1] EK, TP, and IR are first authors.

https://doi.org/10.1016/j.bios.2022.114123
Received 21 December 2021; Received in revised form 12 February 2022; Accepted 20 February 2022
Available online 1 March 2022

glucose monitoring format both interesting and impactful for this study.

In our previous work, *ca.* 0.5 μL of interstitial fluid was typically extracted with MHD into a larger electrolyte volume, which was then analyzed using a spectrophotometric assay (Hakala et al., 2021). In this work, we integrated MHD extraction with the electrochemical detection of glucose due to the following advantages over optical techniques. Using electrodes both to extract and to detect an analyte reduces the device footprint compared with the optical techniques, which require the construction of tightly specified optical paths, a light source, and a detector. Chronocoulometry and chronoamperometry are established methods that routinely yield a detection limit of 0.2–5 μmol/L for glucose with a dynamic range from 5 μmol/L to 20 mmoL/l (see ref. in Table S 2). The concentration of glucose extracted with MHD is 30–140 μmol/L (Hakala et al., 2021) for the porcine skin model and may be lower for human skin. Consequently, electrochemical techniques match the required analytical performance imposed by the extraction method. Finally, amperometry allows total consumption of the extracted analyte during each measurement, resulting in restoration of the sampling compartment's initial conditions. On the contrary, optical techniques require fluid and reactant management to achieve accurate measurements. This difference between the two techniques renders an electrochemical biosensor advantageous as it is reusable over multiple extraction cycles.

In classical amperometric analysis, the experiment is carried out in bulk electrolyte solution under controlled convection. In wearable settings, however, diffusion is the major phenomenon of mass transfer. Moreover, due to the low extracted volume, the interstitial fluid must be analyzed at the sampling site to reduce sample dilution. Consequently, a logical way to interface the electrodes for MHD and chronoamperometry with the human skin is to use a solid electrolyte, such as a hydrogel. A hydrogel establishes a liquid contact between the biosensor and the skin, which reduces the necessary extraction energy. The hydrogel creates a viscous environment, which protects GOx from unfolding and denaturation. In specific cases, the hydrogel acts as a size and charge exclusion membrane to separate the analyte from interfering molecules. Several reviews are devoted to materials used as biosensor membranes (Kulkarni and Slaughter, 2016) and hydrogel formulations are described in patents (Tamada et al., 2006). Nonetheless, the molecular interactions between the analyte and the solid electrolyte and their effect on the analytical performance of a wearable MHD device are still insufficiently studied. To fill this gap in knowledge, we chose a range of materials to interface the extraction/biosensor and the skin (Scheme 1) and studied the integration of a solid-state electrochemical biosensor with an MHD extractor of interstitial fluid.

To obtain a versatile material for a wearable biosensor serving both as a biocatalytic layer and skin-sensor interface layer, we functionalized the working electrode with the enzyme. We tried two approaches: physical entrapment of GOx with a suitable polymer matrix used as a reference material, and a novel approach of tethering GOx to a solid carrier as shown in Scheme 1.

There are many methods to physically trap enzyme into a polymer matrix (González-Sáiz and Pizarro, 2001; Sassolas et al., 2012; Sheldon, 2007; Zdarta et al., 2018). Among those, mixing GOx with chitosan and bovine serum albumin (**BSA**) provides a well-documented performance in wearable biosensor formulations (Bandodkar et al., 2015; Imani et al., 2016). The entrapped enzyme was further covered either with a polyacrylamide hydrogel (**PAG**) or with an electrospun polycaprolactone nanofibrous mat (**NF**) saturated with phosphate buffered saline (**PBS** pH **7.4**) to establish electrolytic contact between the enzymatic layer and the skin. PAG has several advantageous properties: it is hydrophilic and dimensionally stable against changes in relative humidity. PAG bears no net charge and generates insignificant electroosmotic drag. The composition of PAG and its effect on solute diffusion has been extensively discussed in the literature (Amsden, 1998; González-Sáiz and Pizarro, 2001; Yankov, 2004). In contrast to the sponge-like structure of PAG, NF provides an open pore structure and thus less restricted mass transport for the analyte.

A drawback of the physical entrapment of the enzyme in a polymer matrix is that the resulting enzymatic layer is formed by microprecipitation. In such a layer, diffusion is restricted, which affects the biosensor's response time and sensitivity. Furthermore, the entrapment matrix does not prevent the enzyme from migration and unfolding which reduces the accuracy of the biosensor. Therefore, we hypothesized that tethering GOx to a nanofibrous mat could reduce protein migration. Immobilization of enzymes onto nanofibrous mats has been reported (Liu et al., 2020) and the main problem of the method appears to be surface-induced denaturation of immobilized biomolecules. To circumvent the surface-induced denaturation of GOx a spacer molecule

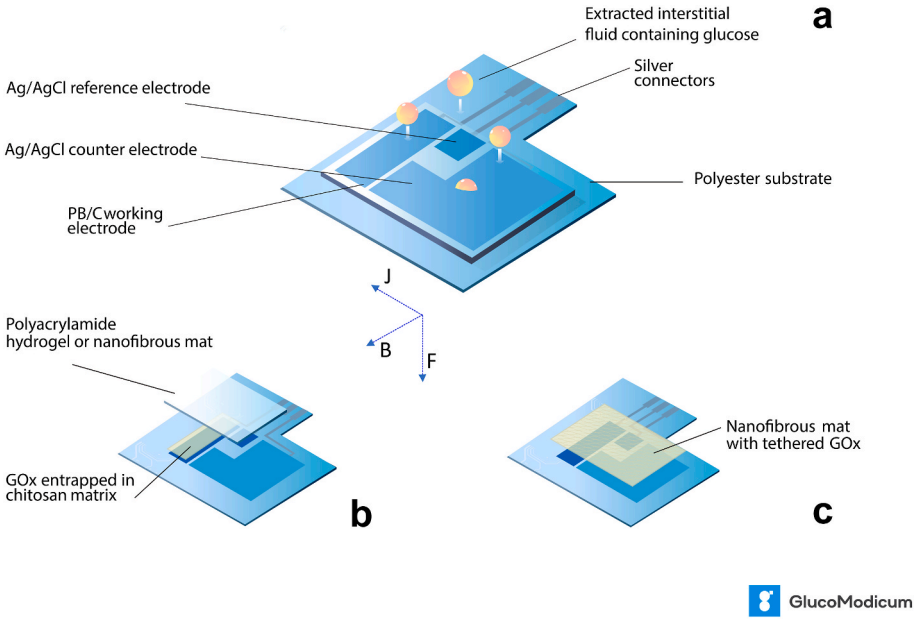

Scheme 1. Elements of the biosensor: (a) A schematic representation of the main parts of the biosensor and flow direction of the extracted interstitial fluid. (b) Two-layered skin-sensor interface created with PAG hydrogel or nanofibrous mat and enzyme layer. (c) Single layer skin-sensor interface where the enzyme tethered on the nanofibrous mat.

is needed between GOx and the nanofiber surface. This can be done with two approaches that we tested: 1) tethering GOx to NF with PEG-di-hydrazide (**Hz-PEG-Hz**) (Scheme S 1), and 2) tethering GOx through avidin-biotin crosslinking (Scheme S 2). The first approach was proven to be a site-specific, mild, and stabilizing modification for proteins (Nischan and Hackenberger, 2014; Ritter et al., 2013). In the second approach, the protein immobilization relies on precipitation of a protein network onto nanofibers. Here, the presence of avidin creates a viscous and crowded environment for GOx and helps maintain its enzymatic activity. We believe that we are the first to report on modification of the nanofibrous mat via site-specific crosslinking of GOx using bifunctional PEG-di-hydrazide and via avidin/biotin co-precipitation for a mild and selective immobilization of GOx on the solid support without significant loss of enzymatic activity.

Finally, we demonstrate that MHD and a biosensor prepared with one of the above-described methods can be combined into a new class of a wearable devices. This approach is the first of its kind demonstrating a safe and efficient way to non-invasively extract glucose through the skin using MHD integrated with chronoamperometric analysis.

2. Experimental

2.1. Chemicals and materials

1-Ethyl-3-(3'-dimethylaminopropyl)carbodiimide hydrochloride (**EDAC HCl**, Merck, 341006), glucose oxidase obtained from *Aspergillus niger*, Type X–S, lyophilized powder, 100,000–250,000 units/g solid (without added oxygen) (**GOx**, Sigma-Aldrich, G7141), sodium periodate ($NaIO_4$, Sigma-Aldrich, MKCJ0321), ammonium sulphate ($(NH_4)_2SO_4$, Sigma-Aldrich, A4418), homobifunctional hydrazide derivative of monodisperse polyethylene glycol (**Hz-PEG-Hz**, 5 kDa, Nanocs, PG2-HZ-5k), sodium cyanoborohydride ($NaCNBH_3$, Sigma-Aldrich, STBH8291), sodium hydroxide (NaOH, VWR BDH Prolabo Chemicals, 28244.295), ethanolamine (Merk, 8.00849), avidin from egg white, lyophilized powder (Sigma-Aldrich, ⩾ 98% (SDS-PAGE) A9275), D(+)-Glucose (Merck, ⩾97.5%, 1,08337), sodium phosphate monobasic monohydrate ($H_2NaPO_4{\cdot}H_2O$, ≥ 99%, Sigma-Aldrich, 71504), sodium phosphate dibasic (HNa_2PO_4, Sigma-Aldrich, 71640), sodium chloride (NaCl, Fisher Chemical, 10428420), Biotin Glucose Oxidase conjugated (**bGOx**, Rockland Immunochemicals, Inc., USA, B000-07) were used without additional purification. Nanofibrous mats (**NF**, custom made polycaprolactone Cellevate Nanomatrix™, 30 μm, Cellevate Ltd., Sweden) were washed with ethanol after electrospinning. All aqueous solutions were prepared using deionized (**DI**) water that was obtained from a water purification unit Barnstead Pacific TII 20 UV, Thermo Scientific.

Phosphate buffered saline (**PBS** pH **7.4**, 10 mM, NaCl 0.138 M; KCl 0.0027 M in pouches, Sigma-Aldrich, P3813) was prepared by dissolving the pouch contents in 1 L of DI water. Phosphate buffered saline (**PBS** pH **6.0**, 10 mM, NaCl 0.138 M; KCl 0.0027 M) was prepared by dissolving 0.19435 g of HNa_2PO_4, 1.191 g of $H_2NaPO_4{\cdot}H_2O$, 8 g of NaCl, and 0.2 g of KCl in 0.8 L of DI water. The obtained buffer was adjusted with NaOH to pH 6.0 and brought up to 1 L with DI water. 5 mM Phosphate buffer (**PB** pH **5.6**) was prepared by dissolving H_2NaPO_4 in DI water and titrating to pH 5.6 with 1 M solution of NaOH. A 0.1 M glucose stock solution was prepared by weighing 18.02 mg of D(+)-glucose in a 1 mL volumetric flask and by dissolving in PBS pH 7.4. The stock solution was left to equilibrate overnight at 4 °C before being used for subsequent dilutions.

2.2. Apparatus and equipment

RF plasma sterilizer (Harrick Plasma Ltd.), 200 W, 0.9 A, connected to Ar gas line was used to pre-treat the electrospun nanofibrous mats. To pre-treat the nanofiber mats, they were put in a Petri dish that was placed into the quartz chamber of the sterilizer. The chamber was closed and rinsed with Ar for 3 min. Next the oil pump was switched on and the chamber was force rinsed with Ar for another 3 min. Then the gas line was closed, the pressure in the sterilization chamber was reduced and the RF plasma was switched on at medium power corresponding to 4 mW/cm^3. The treatment continued for 3 min, the power was switched off and the chamber was filled with Ar.

All electrochemical experiments for biosensor characterization (chronoamperometry) were performed using a MultiEmStat3+ potentiostat from PalmSens BV (The Netherlands) equipped with 4 galvanically isolated channels. Shielded cables from PalmSens BV, with 2 mm banana connectors and crocodile clips, were used to connect the sensors to the potentiostat.

For MHD extraction, a current source Keithley 225 was used in addition to the potentiostat. To extract, the cables of the current source were connected to the leads of the counter electrodes of the setup in Fig. 1. The extraction was carried out for 180 s with a current density of 300 $\mu A/cm^2$ and a magnetic field was created with NdFeB magnets (Supermagnete, Germany) that was measured with a magnetometer AC/DC Magnetic Meter, PCE-MFM 3000 and that was adjusted to 300 mT.

2.3. Sensor manufacturing

Sensors were custom manufactured by LanPrintec Ltd., Spain, on a WT16 polyester substrate with conductive silver traces C2130809D5, dielectric D2080121P12, and carbon mediator C2070424P2, all from Sun Chemical Inc., using screen-printing technology (Fig. 1).

2.4. Biosensor preparation

2.4.1. Nanofiber preparation

NF was used as received or treated with collagen for further hydrophilization. For collagen treatment, NF was placed in a Petri dish; 1 mL of DI water was cast across the entire surface of NF, and the Petri dish with NF was placed in a desiccator under reduced pressure overnight to remove air bubbles from the interfibrillar space of the NF. Then the surface of the NF was blotted to remove excess deionized water and 0.1 ng/mL solution of collagen in DI water was poured over the NF and kept overnight. Non-adsorbed collagen was removed by washing the NF with 3 × 1 mL PBS pH 7.4.

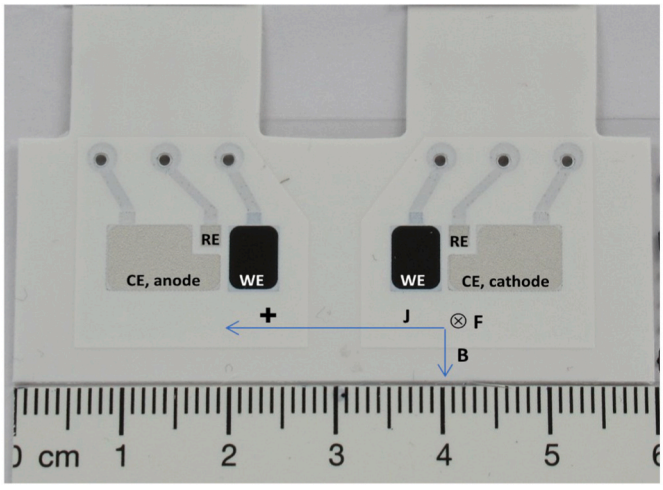

Fig. 1. Electrochemical setup for alternating extraction and analysis of interstitial fluid using magnetohydrodynamics and chronoamperometry. CE is the counter electrode for the biosensor and extraction electrode for MHD extraction, RE is the reference electrode, and WE is the working electrode for the biosensor. **J** is current density, **B** is magnetic field, **F** is Lorenz force.

2.4.2. Tethering GOx to nanofiber

a. Via bifunctional hydrazide-PEG

NF was pre-treated with RF Ar plasma (see Section 2.2). After pre-treatment, a 3.3 × 4.5 cm^2 fragment (8.46 mg) of NF was cut from a larger piece of NF, placed in a Petri dish, pre-wetted with DI water, and was left to dry. 110.7 mg of EDAC HCl was mixed with 2.2 mL of PBS pH 6. Next, 3.3 mL of PBS was added onto the NF followed by adding 2.2 mL of EDAC solution in PBS pH 6 to completely cover the NF with liquid. Finally, the NF was placed in a vacuum desiccator for 3 h to remove air bubbles from the interfibrillar space and to let it react with EDAC.

6.60 mg of GOx was dissolved in 1.980 mL of PBS pH 7.4. 9.46 mg of sodium periodate was dissolved in 220 μL of DI water and protected from light. Enzyme solution was immediately added to the periodate solution, briefly mixed, protected from light, and then left to react for 1 h. After that, the reaction was stopped by adding 2.25 μL of glycerol and by mixing the resulting solution on an orbital shaker for 10 min. The activated protein was purified with a Zeba™ desalting chromatography cartridge (Thermo Fisher, 89934, 1 mL, 7 kDa MWCO) equilibrated with PBS pH 6. All purified protein fractions were collected into the same container.

The Petri dish with NF mat was removed from the vacuum desiccator, EDAC HCl solution was decanted, and the NF was rinsed with 3 × 5 mL of PBS pH 6. Excess liquid in NF was removed with Kimtec™ tissue and purified, oxidized GOx was poured over the NF in the Petri dish. The enzyme was left to react and to bind to NF for 20 min under rocking on the orbital platform, protected from light. The protein was then precipitated by adding ammonium sulphate (Sigma-Aldrich, A4418) to the Petri dish with NF to obtain a saturated solution and to provide uniform coverage of the nanofibers with protein. 18.82 mg of Hz-PEG-Hz was dissolved in 1095.6 μL of PBS pH 7.4 and was added to NF with adsorbed GOx and left to react. After 2 h, 44 μL of 5 M sodium cyanoborohydride (48.45 mg in 154 μL of 1 M NaOH) was added. The reaction system was left to react for 30 min, protected from light. Next, 220 μL of 1 M ethanolamine in DI water was added. After 30 min, NF was washed with 1 × 20 mL and 2 × 15 mL of PBS pH 7.4 and was placed into 15 mL of fresh PBS pH 7.4 overnight to remove the residual cyanide from the final product. Finally, the resulting nanofiber with tethered PEG-GOx was washed with 3 × 15 mL of PBS pH 7.4, dried and then stored at −18 °C until further characterization and use.

b. Via avidin-biotin interaction

Prior to modifying the NF with bGOx, the buffer solution (0.05 M sodium phosphate, 0.75 M NaCl, pH 7.2) of the reconstituted enzyme was replaced with a new buffer of PBS pH 7.4. To do this, the desalting column (Pierce Zeba Desalting Chromatography Cartridges, 7K MWCO, 1 mL, 89934) was equilibrated with PBS pH 7.4 by passing 3 × 3 mL of PBS pH 7.4 at a rate of 1 mL/min 500 μL aliquots of bGOx were passed through the column, flushed with 3 mL PBS pH 7.4, and were collected in fractions of 200 μL. The protein fractions were combined and lyophilized.

Prior to synthesis, the nanofiber mat was collagenated as per section 2.4.2. After that, 27.8 μL of 1 mg/mL avidin solution was drop cast per 1 cm^2 of NF. The mat was then incubated in avidin solution for 4 h (Woo et al., 2003) in a humidity chamber (100% RH) at room temperature on an orbital platform at slow speed. Non-adsorbed avidin was removed by washing with 3 × 1 mL PBS pH 7.4. Lyophilized bGOx was reconstituted in DI water. A volume of bGOx solution at 4.6 μL per cm^2 was drop cast on the nanofiber mat surface. The nanofiber mat was incubated in bGOx solution for 4 h in a humidity chamber at room temperature on an orbital platform at slow speed. Non-adsorbed bGOx was removed by washing with 3 × 1 mL 5 mM PB (pH 5.6). The modified nanofiber was dried and stored in a sealed container with a small amount of desiccant at 4 °C until further use.

2.5. Biosensor characterization

2.5.1. In vitro chronoamperometric calibration

The biosensors with GOx tethered to NF were rinsed with 1 mL PBS pH 7.4 and then air-dried. The biosensors with entrapped enzyme used as is. The biosensor electrodes were connected to the potentiostat, the biosensor was placed in a humidity chamber, and 50 μL of PBS pH 7.4 was added to the biosensor surface to cover WE, RE, and CE - and to act as a liquid cell for calibration. Chronoamperometry was performed with an applied potential of 0.0 V. The time interval between recorded current values was 1 s. Additions of glucose were performed following the protocol outlined in Table S 3, recording the time of each addition. An addition of glucose was made when the measured current had reached a stable minimum.

The raw data obtained from the chronoamperometric measurements were graphed using Origin 2020b (OriginLab Corporation) to show the current response *vs.* time. The raw data was first smoothed with the Signal Processing tool in the Origin package using a Savitzky-Golay filter with polynomial order 1, no boundary condition, and with 10–50 points to remove the peak-to-peak noise without losing the shape of the responses to glucose. The response data points were identified as the stabilized current values following an addition of a glucose aliquot (Table S 3). The response data point values and glucose concentrations were used to perform a linear regression analysis. The linear fit parameters as well as the time to reach a stabilized current were used to determine the sensitivity of the biosensor (slope of the linear fit), linearity (analysis of residuals), goodness of fit (R^2), and response time. The parameters of all electrodes tested within a batch were averaged and the standard deviation was calculated.

2.5.2. Extraction and measurements of glucose through excised porcine skin using integrated MHD and biosensor electrodes

Pig ears were obtained from a local slaughterhouse (Kiven säästöpossu, Karkkila, Finland). After pig slaughter, the ears stayed 2 h at 20 °C due to specifications of the slaughtering process and were then transported in a refrigerated vehicle for 1 h to the laboratory. Upon arrival, the ears were washed with cold running tap water and rectangular skin samples of 2 × 5 cm^2 and 500–800 μm thick were dissected from the outer/dorsal surface of each ear with a dermatome (Nouvag TCM 3000 BL, Nouvag, Switzerland). The individual skin samples were wrapped in paraffin film (Parafilm® PM996, Bemis Company, Inc.) and stored in a freezer at −20 °C until use. The samples were used within 3 months from dissecting. Before the experiments, the skin samples were thawed to room temperature (22 °C) and were washed three times for 30 min in PBS pH 7.4. Extra solution on the skin surface was wiped with paper tissue (Kimtech™ wipe).

2% agarose gels were prepared by dissolving 0.5 g of agarose (Top-Vision, ThermoFisher Scientific) in 25 mL of PBS pH 7.4 and bringing the slurry to boiling on a hot plate under constant stirring. For the agarose gels with glucose, agarose was dissolved in 1 or 3 mM glucose solution in PBS pH 7.4. After the boiling solution of agarose became clear, 12 mL of the gel was cast in a cell culture dish with an electronic pipette controller and was allowed to cool down to room temperature before storing in a fridge at 4 °C until use.

For the *ex vivo* experiments, the biosensor and magnet were placed on top of the skin sample and the resulting stack was placed on the agarose gel. The measurement was immediately started upon placement on the skin and followed by a consecutive cycle of amperometry and MHD extraction. The polarity of the MHD extraction was alternated. To change glucose concentration, the measurement was paused, and both the skin and the MHD/biosensor setup were transferred onto the next agarose gel in the following order: 0, 1, 3 and the initial 0 mM glucose gels.

3. Results

3.1. Tethering GOx to the nanofibrous mat and its effect on ***in vitro*** analytical performance of the biosensor

Fig. 2 a,b shows point calibration plots of biosensors having a nanofibrous mat with immobilized GOx welded over WE, RE, and CE. Fig. 2 c compares the sensitivity of each type of biosensor calculated from the slopes of point calibration curves. Fig. 2 d compares the response time of each type of the biosensor calculated as the time required for biosensor response to stabilize after adding an aliquot of glucose solution. Due to the expected range of glucose concentrations in the model of interstitial fluid being 30–140 μM and because we expected the concentration to be lower for human skin, the study focused on the concentration range 0.2–25 μM.

The *in vitro* analytical performance of the biosensors prepared by tethering GOx to a nanofibrous mat are summarized in Table S 1, Table 1 and are compared with biosensors prepared with the entrapment method (see Supporting information, Figures S 1-S 4).

3.2. Storage stability

Glucose biosensors prepared by the physical entrapment method generally lack stability and exhibit drift of response current when stored (Lin et al., 2019). In this study, the largest current fluctuations (and highest noise level) of such biosensors manifested during the first 48 h after placing PAG hydrogel on the enzymatic layer (Fig. S 5). We associate the instability of the amperometric response with enzyme diffusion inside the hydrogel matrix since the hydrogel acquires enzyme-specific coloration. After 48 h of storage the biosensors were stable for at least 6 months without exhibiting significant fluctuations in analytical performance (Fig. S 6).

When the nanofibrous mat was used to interface the skin and the biosensor, no fluctuations in amperometric response were observed, and the biosensors were ready to use right away. The biosensor having GOx tethered to the nanofibrous mat via avidin-biotin interactions gradually deteriorated losing 43% of its initial sensitivity over the first 8 weeks (Fig. 3 b). The biosensor with GOx tethered to the nanofibrous mat by PEG-di-hydrazide crosslinker was stable and showed no statistically significant difference between sensitivity values over the studied 8-week period (Fig. 3 a).

3.3. Magnetohydrodynamic extraction and amperometric detection of glucose through ***ex vivo*** porcine skin

Fig. 4 a-c shows the results of MHD extraction of the model fluid (solution of glucose in PBS pH 7.4) through excised porcine skin with alternating amperometric analysis and MHD extraction. At t = 0 s the skin placed on an agarose gel slab saturated with PBS pH 7.4 (point indicated as 0 mM in Fig. 4 a-c) and then the biosensor was immediately placed on top of the skin-gel stack to start the measurement. The MHD extraction was done between the amperometric measurements, resulting in the data pattern shown in Fig. 4 d, where the time gap between two adjacent amperometric measurements corresponds to the duration of MHD extraction. Each amperometric curve in Fig. 4 a-c started with a negative current spike, then the current quickly stabilized. The amperometric response to 0 mM glucose concentration provided a baseline for the subsequent measurements. This baseline response accounts for all effects caused by or associated with the skin properties, the extraction current, and the magnetic field at the system level. After achieving a stable amperometric response to the 0 mM glucose concentration, the gel slab underneath the skin was replaced with another agarose gel slab saturated with 1 mM glucose solution in PBS pH 7.4 (arrows with 1 mM annotation, Fig. 4 a-c), and the measurement cycle of amperometry and MHD extraction was immediately resumed. Fig. 4 a-c shows that the values of the stabilized part of the current appear to be significantly more negative after replacement of the gel. The control experiment without GOx in the formulation (Fig. 4 e) generated a different magnitude of current changes. Therefore, the change in amperometric response correlates with change in glucose concentration. After

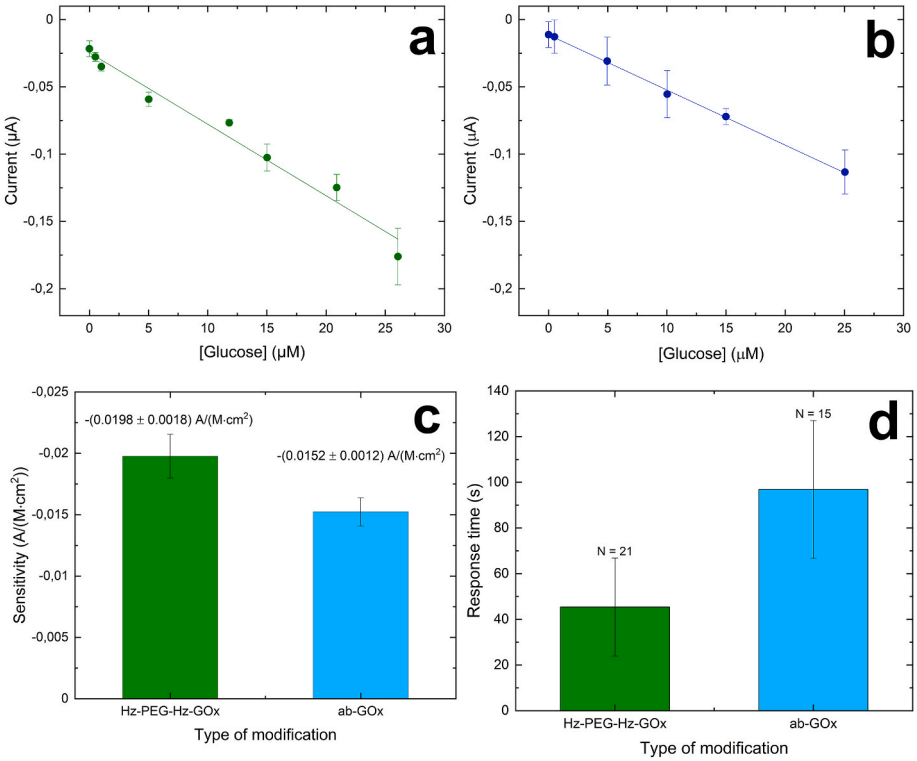

Fig. 2. Point calibration curves for biosensors with GOx tethered to a nanofibrous mat (a, green) via bifunctional PEG-di-hydrazide (**Hz-PEG-Hz-GOx**) and (b, blue) via avidin/biotin interactions (**ab-GOx**), their calculated (c) sensitivity, and (d) response time. Error bars in a-c are reproducibility standard deviation (N = 3).

Table 1
Analytical performance of the biosensors and system (biosensor and MHD extractor).

Sensor	N	-Sensitivity (A M^{-1} cm^{-2})		Drop factor[a]	Recovery to initial current (%)
		Integrated system	Biosensor		
145 μm PAG	4	$(6.80 \pm 0.36) \times 10^{-4}$	$(1.4 \pm 0.5) \times 10^{-2}$	21	97 ± 2
NF-Hz-PEG-Hz-GOx	4	$(8.97 \pm 0.35) \times 10^{-4}$	$(1.98 \pm 0.18) \times 10^{-2}$	22	88 ± 14
NF-ab-GOx	4	$(7.28 \pm 0.27) \times 10^{-4}$	$(1.52 \pm 0.12) \times 10^{-2}$	22	96 ± 4
Sensor ↓	**Response time (s)[b]** ***Integrated system***				***Biosensor***
Glucose concentration →	**0 mM**	**1 mM**	**3 mM**	**0 mM**	**1–25 μM**
145 μm PAG	1050 ± 250	700 ± 250	700 ± 600	2700 ± 1050	220 ± 130
NF-Hz-PEG-Hz-GOx	350	1400	700	>3500	45 ± 21
NF-ab-GOx	1225 ± 880	875 ± 180	700 ± 0	2800 ± 350	100 ± 30

[a] Drop factor – coefficient of decrease in biosensor sensitivity tested in *ex vivo* conditions compared with its sensitivity *in vitro*. '21' corresponds to a 95% drop.
[b] A response time to 0 mM glucose is the average time to reach a stable and reproducible current.

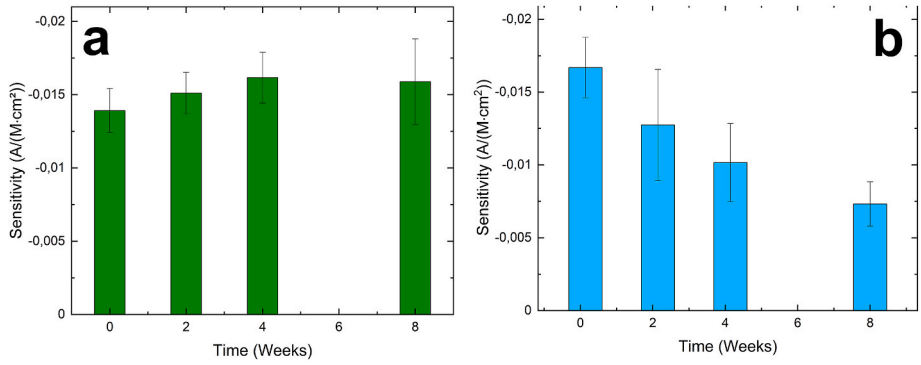

Fig. 3. Shelf-life study of biosensor (a, green) with nanofibrous mat and GOx tethered via Hz-PEG-Hz crosslinker and (b, blue) with nanofibrous mat and GOx tethered via avidin-biotin interactions, both stored at 4 °C and 100% of relative humidity (**RH**), N = 4.

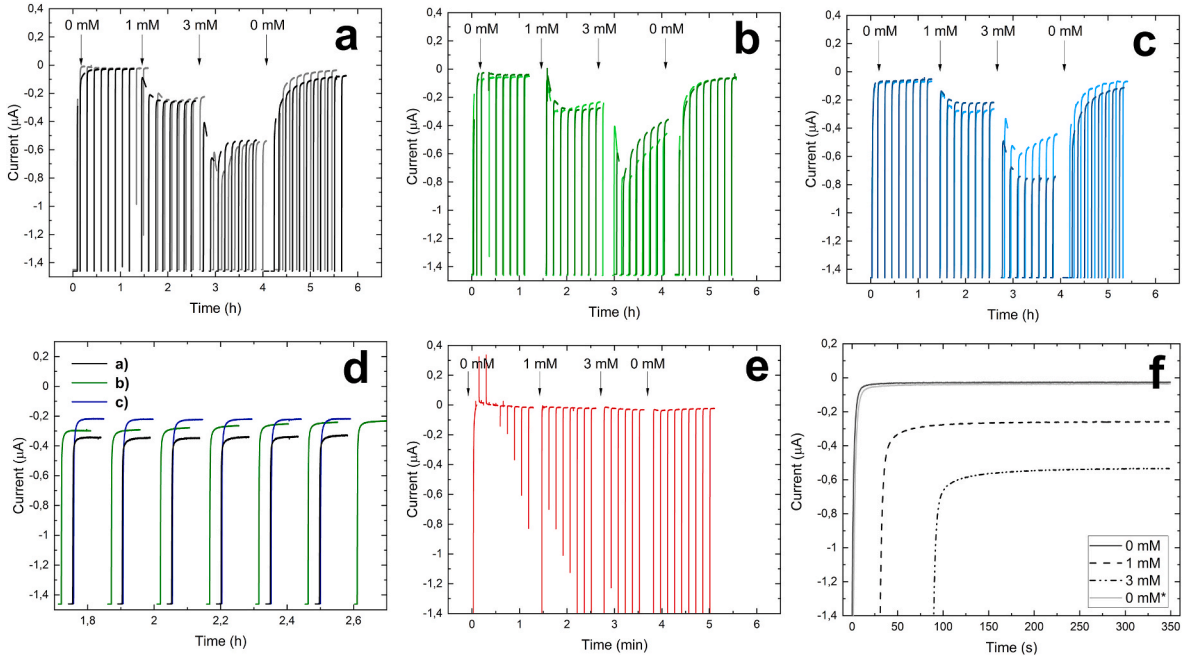

Fig. 4. Amperometric measurements of glucose extracted through excised porcine skin using the MHD technique with two individual biosensors having (a, grey) GOx entrapped in chitosan and overlaid PAG as the skin-biosensor interface, (b, green) nanofibrous mat with GOx tethered via PEG-di-hydrazide crosslinkers, and (c, blue) nanofibrous mat with tethered GOx via avidin-biotin interaction. (d) Comparison between a, b, and c (exploded view, corresponding colors) at glucose concentration 1 mM, (e) control experiment with sensor having no GOx, and (f, grey) biosensor (PAG hydrogel based) response as a function of glucose concentration under the porcine skin, where the selected curves are those from (a) immediately prior to replacing the agarose gel of known glucose concentration with a new gel. 0 mM* is the gel containing no glucose used after the gel containing 3 mM glucose in order to test the biosensor recovery.

replacing the gel containing 1 mM glucose solution with a gel with 3 mM solution of glucose, the values of the stabilized current decreased further. Finally, the current returned to baseline when the gel slab was replaced by one containing no glucose. The end-point biosensor response to each glucose concentration in agarose gel is shown in Fig. 4 f.

To understand the effect of the skin barrier on the biosensor performance we calculated an apparent sensitivity of the integrated system (the biosensor and MHD extractor) by taking the end points of the stabilized part of the current in Fig. 4 a-c for each glucose concentration (Fig. S 9, Table S 5) and comparing it with the analytical performance of the biosensors as per Table S 1. The data are summarized in Table 1, column Integrated system corresponds to the tests *ex vivo*.

Table 1 indicates that the apparent sensitivity to glucose of the device with integrated biosensor and MHD extractor is 4–5% of the benchmark analytical sensitivity of the biosensor.

4. Discussion

4.1. General considerations that guide the biosensor design and its integration with MHD extractor

4.1.1. Mass transfer at the biosensor

The net rate of electrochemical reaction (ν_{rxn}) is determined by the rate of mass transfer (ν_{mt}) at the electrode:

$$\nu_{rxn} = \nu_{mt} = \frac{i_t}{nFA} \tag{1}$$

where i_t is observed current, n is stoichiometric number of electrons involved in the electrochemical reaction, F is Faraday's constant, and A is the area of working electrode. The mass transfer rate ν_{mt} (1) at a distance x from the working electrode surface can be expressed as a flux of the reactive species i (H_2O_2) through an area A:

$$J_i(x) = -D_i\frac{\partial C_i}{\partial x} - \frac{z_i F}{RT}D_i C_i\frac{\partial \varphi_i}{\partial x} + C_i v(x) \tag{2}$$

where D_i is the diffusion coefficient of species i, $\frac{\partial C_i}{\partial x}$ is its concentration gradient at distance x, and $\frac{\partial \varphi_i}{\partial x}$ is its potential gradient, z_i is the charge of the species and C_i is its concentration, R is the universal gas constant, T is temperature, and $v(x)$ is the velocity of a volume element in solution moving along the axis. The terms in the equation describing the flux determine diffusion ($-D_i\frac{\partial C_i}{\partial x}$), migration ($-\frac{z_i F}{RT}D_i C_i\frac{\partial \varphi_i}{\partial x}$), and convection ($C_i v(x)$), respectively. The reactive species i is hydrogen peroxide as it is the only one undergoing electrocatalytic conversion in the system under investigation. Wearable devices often operate with small volumes of extracted interstitial fluid; thus, convection is only possible due to a temperature gradient in the space between the skin and wearable device. The skin-sensor interface layer is typically thin, up to 500 μm, and the use of water-based hydrogels provides high heat transfer rate and rapidly achieves temperature equilibrium between the biosensor and the subject's skin. Moreover, the use of hydrogel makes it practically difficult to mix the fluid by means of convection. Thus, one can disregard the convection term. Because the skin-sensor interface layer contains PBS pH 7.4 as supporting electrolyte with ionic strength 0.154 M, one can neglect the migration term as well. In this way, the performance of the wearable electrochemical biosensor is determined by diffusion of hydrogen peroxide:

$$J_{H_2O_2}(x) = -D_{H_2O_2}\frac{\partial C_{H_2O_2}}{\partial x} \tag{3}$$

4.1.2. Mass transfer with MHD

Upon MHD extraction, the equation for the flux of glucose $J_{glucose}(x)$ or hydrogen peroxide $J_{H_2O_2}(x)$ through an area A of the skin-sensor interface layer can be used. In addition to the diffusion term, electrokinetic and magnetohydrodynamic terms now also describe the flux. Both glucose and hydrogen peroxide bear no ionic charge and thus they can be carried to the electrode surface by the electroosmotic flow, U_{EOF}, occurring in the *stratum corneum* and skin-sensor interface layer when an electric current is applied.

$$U_{EOF} = \frac{-\varepsilon\zeta_0 E}{\eta} \tag{4}$$

The electroosmotic flow U_{EOF} is determined by ζ_0 – the zeta potential of the pore wall, ε – the relative dielectric permittivity of interstitial fluid, E – the strength of the electric field, and is inversely proportional to dynamic viscosity of the fluid η. The MHD term for interstitial fluid is proportional to the magnetic field, the current density, the fluid's electric impedance, and inversely proportional to the fluid viscosity. Electromigration terms only appear during MHD extraction of interstitial fluid.

4.1.3. Diffusion in bulk electrolyte and porous medium

After MHD extraction, the rate of the mass transfer of glucose and hydrogen peroxide in the skin-sensor interface layer is proportional to their diffusion coefficients:

$$D = \frac{RT}{N_A 6\pi\eta R_h} \tag{5}$$

where R is the universal gas constant, T is temperature, N_A is Avogadro's constant, η is the dynamic viscosity of the electrolyte, and R_h is a hydrodynamic radius of the molecule of interest. Thus, in all cases, the upper limit for the current obtained in such systems is dictated by the dynamic viscosity of the electrolyte used in the theoretical analysis. However, in practical conditions of wearable devices, when hydrogels or other porous materials are used, the apparent diffusion D_e is determined by the material properties (Weissberg, 1963), such as porosity ε_t, constrictivity δ, and tortuosity τ, which may increase the path length that the species need to travel:

$$D_e = \frac{D\varepsilon_t\delta}{\tau} \tag{6}$$

Although the latter equation and the continuum scale approach has been criticized for its empirical nature, it is relevant for describing the diffusion of solutes in a liquid confined in a porous environment. Besides the continuum scale model, more sophisticated ones (Amsden, 1998) can be used for approximating hydrogels as a soft expandable network with short (nm scale) crosslink segments (segments of macromolecule between two crosslinks) and nanofibrous mats as a hard non-deformable network with crosslink segments of fibers on the scale of upper tens or hundreds of nm. According to these models (Amsden, 1998), the diffusivity of the analyte in a hydrogel may be affected by structural parameters of the hydrogel, such as degree of crosslinking, mobility of the polymer chains, presence of charged groups, pore connectivity *etc*. Thus, structural parameters of the skin-sensor interface must be considered when optimizing analytical performance of a wearable device.

4.2. Effect of structural parameters of the skin-biosensor interface layer on the analytical performance of the biosensor

To understand whether the structural parameters of the hydrogel and nanofiber may affect the analytical performance of the biosensor, we estimated the pore size of the PAG using available literature (Holmes and Stellwagen, 1991; Schultz and Solomon, 1961; Stellwagen, 1998). The most common composition of PAG in this work is 10% of total monomer concentration (**%T**), and 0.5–2% of crosslinker (**%C**). The pore radius of PAG with this composition (110-70 nm) is 170–260 times larger than the radius of glucose molecules ($R_h = 0.42$ nm). The pores of nanofiber mats are formed from randomly aligned filaments of

polycaprolactone, and their radius is from 0.1 to 2.5 μm (Fig. S 7). This way, the pore radius for both materials is substantially larger than the mean free path of glucose and hydrogen peroxide, *i.e.,* movement of analyte within the pores may be close to the diffusion in the bulk solution.

4.2.1. Tortuosity and constrictivity

The data in Fig. S 1a and in Fig. S 3 suggest no statistically significant difference in sensitivity between biosensors with PAG of different thicknesses. The response time, on the contrary, indicates that PAG obstructed the analyte diffusion when the gel thickness exceeded 700 μm and at high total monomer (**%T**) and crosslinker (**%C**) concentrations in the hydrogel, *i.e.*, when the polymer network is dense. In other words, due to the large pore size of PAG, tortuosity is a major limiting parameter that impedes the diffusion of the analyte (Elwinger et al., 2017) in the skin-biosensor interface layer. Only at %T $\geq$ 33% and %C $\geq$ 1.5% does the pore diameter, *i.e.*, constrictivity, influence the response time. In this way, the thinner the interface layer between the skin and the biosensor, the closer the apparent diffusion coefficient of analytes is to their diffusion coefficient in bulk solution. Thus, it is reasonable to expect that a 30 μm thick nanofibrous mat with its open pore structure may improve the response time of the biosensor compared to polyacrylamide hydrogel. Indeed, when a nanofibrous mat was used instead of PAG to overlay GOx trapped in chitosan, both the sensitivity and the response time improved significantly: the relative standard deviation of the sensitivity decreased from 50% to 8.2%, the mean sensitivity increased from −0.034 to −0.085 A/(M·cm^2), and the response time decreased from 133 s to 17 s (Figure S 1, S 2 and Table S 1).

4.2.2. Solvent viscosity

We studied the effect of solvent viscosity (see Supporting Information, Fig. S 4) by adding glycerol to PBS pH 7.4 used to prepare the skin-sensor interface. Figure S 4a shows a slight improvement in sensitivity of the biosensor with PAG containing 15% glycerol. This improvement can be attributed to glycerol stabilizing the enzyme folding by creating a crowded environment similar to a native one (Harris et al., 2013; Vasileva and Godjevargova, 2005). Apart from the improved sensitivity, such a biosensor had a significantly slower response time: 340 s *vs.* 150 s compared to a sensor with PAG in pure PBS pH 7.4 (Fig. S 4c).

The response time of the biosensor interfaced with the nanofibrous mat also increased from 60 s in pure PBS pH 7.4 to 120 s in PBS pH 7.4 containing 15% of glycerol. In contrast to the biosensor with PAG, the sensitivity of the biosensor with nanofibrous mat decreased when glycerol was added (Fig. S 4b,d), which contradicts the known literature. Interestingly, the same biosensor recovered its sensitivity once the PBS-glycerol mixture was replaced with pure PBS pH 7.4. We speculate that the observed phenomenon may be an inactivation of the enzyme caused by its absorption onto nanofibers. There are several possible mechanisms for how the inactivation could occur (Faulón Marruecos et al., 2018; Haynes and Norde, 1994). One potential cause may be the dehydration of a protein at a hydrophobic surface, as polycaprolactone is more hydrophobic than polyacrylamide. However, the investigation of this hypothesis is outside the scope of the present study.

In summary, among the parameters of the skin-biosensor interface layer, only the solvent viscosity has a major effect on the biosensor performance. Structural features of the interface layer, such as constrictivity and tortuosity, affect the response time of the biosensor only if the interface layer is thick (over 700 μm) or dense (%T = 33%). Neither of these cases are important in practice. It should be noted though that interface inhomogeneity may be a major source of large standard deviation of the analytical sensitivity of the biosensor and hence should be strictly controlled.

4.3. Effect of tethering enzyme to a nanofibrous mat

Considering the effects that the structure of the skin-sensor interface layer has on the analytical performance of the biosensor, we hypothesize that the interface layer should be as thin as possible and that it should have an open pore structure, like in a nanofibrous mat. Such a design should provide a bulk-like diffusion of analytes across the interface layer. However, in this case, modification of the sensor with an enzyme must be done in a different way than by entrapment. The drawback of entrapment of the enzyme in the nanofiber or another polymer is a gradual migration of the enzyme from the entrapment matrix. Tethering the enzyme to the nanofibrous mat (Fig. S 7) offers negligible rates of protein migration (Table S 4) even in a strong electromagnetic field. Producing the enzyme-modified nanofibrous mat is straightforward and scalable. Sensor modification with the modified NF mat can be done by welding it to the sensor substrate over the three-electrode setup to ensure alignment. The results in Fig. 2, Table S 1, and Table 1 suggest a faster response time and increased accuracy when compared with the hydrogel-based biosensors. The in-use stability (Fig. 3) suggests that the biosensor based on a nanofibrous mat modified with GOx via a PEG-di-hydrazide crosslinker can be re-used multiple times during 8 weeks without a statistically significant loss of activity.

4.4. Integration of the biosensor and MHD extractor for detection of glucose levels through an ex vivo skin model

We utilized *ex vivo* porcine skin to simulate a wearable sensor in a situation where the emphasis is on low blood sugar levels (Fig. 4). The glucose concentration in human interstitial fluid is similar to that in blood plasma (Cengiz and Tamborlane, 2009), ranging from 2 to 16 mM. The most dangerous glucose levels are typically below 3 mM that might cause seizures and death if untreated. The relevance of porcine skin as a model for human skin has been discussed in the literature (Moniz et al., 2020; Schmook et al., 2001; Sieg et al., 2003). In brief, porcine skin features an isoelectric point, a vascular density, and a permeability close to those of human skin. Porcine skin has few hair follicles and is generally superior to *in vitro* reconstructs of human skin. However, the permeability of porcine skin is 2–2.5 times higher than that of human skin (Dick and Scott, 2011). Consequently, the glucose levels between 1 and 3 mM tested in the *ex vivo* setup using the porcine skin model would correspond to a clinically relevant range 2–7.5 mM of glucose in human skin.

All our biosensors demonstrated high correlation of the amperometric response with glucose concentration underneath the skin. We evaluated the biosensor recovery, apparent sensitivity, and response time. The data are summarized in Table 1. Table 1 and Fig. 4d show that the biosensor speed and the sensitivity *in vitro* do not directly predict the speed and sensitivity of the MHD setup integrated with chronoamperometric analysis in an *ex vivo* setting. The decrease in sensitivity to 4–5% of the sensitivity obtained *in vitro* and the increase in response time recorded in the experiments were caused by the porcine skin that prevents fluid and glucose transport. This skin barrier prolonged the time required to reach a steady current response in the experiment. However, as previously demonstrated (Hakala et al., 2021), the MHD extraction increases the flux of interstitial fluid by 2 times compared to passive diffusion and 13 times compared to the flux created by reverse iontophoresis. This extraction efficiency makes it possible to obtain a large interstitial fluid sample, to minimize sample dilution, and to match the amount of extracted glucose with the dynamic range of the biosensor. The relative standard uncertainty of the integrated extractor and biosensor, tested on an *ex vivo* skin model, did not exceed 5.3%. Together with high extraction efficiency, the low value of uncertainty on the system level indicates that a significant correlation between the glucose concentration in underlying tissue and the biosensor response can be achieved.

5. Conclusions

We demonstrated that the sensitivity, accuracy, response time, shelf-

life, and in-use stability can be significantly improved by optimizing the mass-transfer phenomena at the biosensor-skin interface. The sensor performance was significantly improved by tethering the enzyme to a nanofibrous mat under mild reaction conditions. We showed that the biosensor integrated with the magnetohydrodynamic extraction produced an amperometric response that was correlated with glucose levels present in the skin model system. The effect of the *ex vivo* skin barrier on the analytical performance of the biosensor was quantified and the results point to a possibility to combine magnetohydrodynamic extraction and glucose determination in a wearable device for non-invasive glucose monitoring. The further development of the field of magnetohydrodynamic extraction of interstitial fluid through *human skin* together with an integrated biosensor will result in a new class of a needle- and microneedle-free medical device for glucose monitoring in people requiring diabetes management.

CRediT authorship contribution statement

Emily Kemp: Experimental, Investigation, Methodology, Formal analysis, Investigation, Writing – original draft. **Tommi Palomäki:** Experimental, Investigation, Methodology, Formal analysis, Investigation, Writing – original draft. **Ida A. Ruuth:** Experimental, Investigation, Methodology, Formal analysis, Investigation, Writing – original draft. **Zhanna A. Boeva:** Conceptualization, Methodology, Supervision, Data, Visualization, Writing – original draft, Writing – review & editing. **Teemu A. Nurminen:** Experimental, Investigation, Methodology, Software, Writing – review & editing. **Risto T. Vänskä:** Experimental, Investigation, Methodology, Software, Writing – review & editing. **Laura K. Zschaechner:** Data curation, Formal analysis, and Data Management, Writing – review & editing. **Alejandro García Pérez:** Conceptualization, Resources, Funding acquisition, Writing – review & editing. **Tuuli A. Hakala:** Resources, Methodology, Writing – review & editing. **Melissa Wardale:** Resources, Methodology, Writing – review & editing. **Edward Haeggström:** Funding acquisition, Project administration, Resources, Validation, Writing – review & editing. **Johan Bobacka:** Funding acquisition, Project administration, Resources, Validation, Writing – review & editing.

Declaration of competing interest

A.G.P, R.T.V., T.A.N., Z.A.B., E.H., and J.B. are cofounders of GlucoModicum ltd, which develops technologies and products for needle-free health and biomarker monitoring and holds patents related to the MHD method. T.A.H., A.G.P., M.W., I.A.R., R.T.V., T.A.N., E.K., T.P, L.K. Z., and Z.A.B. are employees of GlucoModicum Ltd. J.-M.A., K. P.-F., E. H., and J.B. are scientific advisors for GlucoModicum Ltd. E.H. and J.B. are members of the GlucoModicum Ltd. board.

Acknowledgements

GlucoModicum affiliates are grateful to Business Finland (projects 2538/31/2018 and 6855/31/2019) for financial support.

Appendix A. Supplementary data

Supplementary data to this article can be found online at https://doi.org/10.1016/j.bios.2022.114123.

References

Amsden, B., 1998. Solute diffusion within hydrogels. Mechanisms and models. Macromolecules 31, 8382–8395. https://doi.org/10.1021/ma980765f.

Bandodkar, A.J., Jia, W., Yardımcı, C., Wang, X., Ramirez, J., Wang, J., Yardimci, C., Wang, X., Ramirez, J., Wang, J., 2015. Tattoo-based noninvasive glucose monitoring: a proof-of-concept study. Anal. Chem. 87, 394–398. https://doi.org/10.1021/ac504300n.

Bandodkar, A.J., Wang, J., 2014. Non-invasive wearable electrochemical sensors: a review. Trends Biotechnol. 32, 363–371. https://doi.org/10.1016/j.tibtech.2014.04.005.

Blum, A., 2018. Freestyle libre glucose monitoring system. Clin. Diabetes 36, 203–204. https://doi.org/10.2337/cd17-0130.

Cengiz, E., Tamborlane, W.V., 2009. A tale of two compartments: interstitial versus blood glucose monitoring. Diabetes Technol. Therapeut. 11 https://doi.org/10.1089/dia.2009.0002. S-11-S-16.

Dick, I.P., Scott, R.C., 2011. Pig ear skin as an in-vitro model for human skin permeability. J. Pharm. Pharmacol. 44, 640–645. https://doi.org/10.1111/j.2042-7158.1992.tb05485.x.

Elwinger, F., Pourmand, P., Furó, I., 2017. Diffusive transport in pores. Tortuosity and molecular interaction with the pore wall. J. Phys. Chem. C 121, 13757–13764. https://doi.org/10.1021/acs.jpcc.7b03885.

Faulón Marruecos, D., Schwartz, D.K., Kaar, J.L., 2018. Impact of surface interactions on protein conformation. Curr. Opin. Colloid Interface Sci. 38, 45–55. https://doi.org/10.1016/j.cocis.2018.08.002.

Garcia Perez, A., Nieminen, H., Haeggström, E., 2019. Device for sampling one or more analytes. Patent FI20195204A1.

González-Sáiz, J.M., Pizarro, C., 2001. Polyacrylamide gels as support for enzyme immobilization by entrapment. Effect of polyelectrolyte carrier, pH and temperature on enzyme action and kinetics parameters. Eur. Polym. J. 37, 435–444. https://doi.org/10.1016/S0014-3057(00)00151-8.

Hakala, T.A., Pérez, A.G., Wardale, M., Ruuth, I.A., Vänskä, R.T., Nurminen, T.A., Kemp, E., Boeva, Z.A., Alakoskela, J.M., Fernholm, K.P., Hæggström, E., Bobacka, J., 2021. Sampling of fluid through skin with magnetohydrodynamics for noninvasive glucose monitoring. Sci. Rep. 1–9 https://doi.org/10.1038/s41598-021-86931-7.

Harris, J.M., Reyes, C., Lopez, G.P., 2013. Common causes of glucose oxidase instability in in vivo biosensing: a brief review. J. Diabetes Sci. Technol. 7, 1030–1038. https://doi.org/10.1177/193229681300700428.

Haynes, C.A., Norde, W., 1994. Globular proteins at solid/liquid interfaces. Colloids Surf. B Biointerfaces 2, 517–566. https://doi.org/10.1016/0927-7765(94)80066-9.

Holmes, D.L., Stellwagen, N.C., 1991. Estimation of polyacrylamide gel pore size from Ferguson plots of linear DNA fragments. II. Comparison of gels with different crosslinker concentrations, added agarose and added linear polyacrylamide. Electrophoresis 12, 612–619. https://doi.org/10.1002/elps.1150120903.

Imani, S., Bandodkar, A.J., Mohan, A.M.V., Kumar, R., Yu, S., Wang, J., Mercier, P.P., 2016. A wearable chemical-electrophysiological hybrid biosensing system for real-time health and fitness monitoring. Nat. Commun. 7, 1–7. https://doi.org/10.1038/ncomms11650.

Kim, J., Campbell, A.S., Wang, J., 2018. Wearable non-invasive epidermal glucose sensors: a review. Talanta 177, 163–170. https://doi.org/10.1016/j.talanta.2017.08.077.

Kulkarni, T., Slaughter, G., 2016. Application of semipermeable membranes in glucose biosensing. Membranes 6. https://doi.org/10.3390/membranes6040055.

Kurnik, R.T., Berner, B., Tamada, J.A., Potts, R.O., 1998. Design and simulation of a reverse iontophoretic glucose monitoring device. J. Electrochem. Soc. 145, 4119. https://doi.org/10.1149/1.1838924.

Lin, Y., Bariya, M., Nyein, H.Y.Y., Kivimäki, L., Uusitalo, S., Jansson, E., Ji, W., Yuan, Z., Happonen, T., Liedert, C., Hiltunen, J., Fan, Z., Javey, A., 2019. Porous enzymatic membrane for nanotextured glucose sweat sensors with high stability toward reliable noninvasive health monitoring. Adv. Funct. Mater. 29, 1902521. https://doi.org/10.1002/adfm.201902521.

Lipani, L., Dupont, B.G.R., Doungmene, F., Marken, F., Tyrrell, R.M., Guy, R.H., Ilie, A., 2018. Non-invasive, transdermal, path-selective and specific glucose monitoring via a graphene-based platform. Nat. Nanotechnol. 13, 504–511. https://doi.org/10.1038/s41565-018-0112-4.

Liu, Yanbo, Hao, M., Chen, Z., Liu, L., Liu, Yao, Yang, W., Ramakrishna, S., 2020. A review on recent advances in application of electrospun nanofiber materials as biosensors. Curr. Opin. Biomed. Eng. 13, 174–189. https://doi.org/10.1016/j.cobme.2020.02.001.

Moniz, T., Costa Lima, S.A., Reis, S., 2020. Human skin models: from healthy to disease-mimetic systems; characteristics and applications. Br. J. Pharmacol. 177, bph.15184. https://doi.org/10.1111/bph.15184.

Nischan, N., Hackenberger, C.P.R., 2014. Site-specific PEGylation of proteins: recent developments. J. Org. Chem. 79, 10727–10733. https://doi.org/10.1021/jo502136n.

Pikal, M.J., 2001. The role of electroosmotic flow in transdermal iontophoresis. Adv. Drug Deliv. Rev. 46, 281–305. https://doi.org/10.1016/S0169-409X(00)00138-1.

Rao, G., Glikfeld, P., Guy, R.H., 1993. Reverse iontophoresis: development of a noninvasive approach for glucose monitoring. Pharm. Res. 10, 1751–1755. https://doi.org/10.1023/A:1018926215306.

Rao, G., Guy, R.H., Glikfeld, P., LaCourse, W.R., Leung, L., Tamada, J., Potts, R.O., Azimi, N., 1995. Reverse iontophoresis: noninvasive glucose monitoring in vivo in humans. Pharm. Res. 12, 1869–1873. https://doi.org/10.1023/A:1016271301814.

Ritter, D.W., Roberts, J.R., McShane, M.J., 2013. Glycosylation site-targeted PEGylation of glucose oxidase retains native enzymatic activity. Enzym. Microb. Technol. 52, 279–285. https://doi.org/10.1016/j.enzmictec.2013.01.004.

Sassolas, A., Blum, L.J., Leca-Bouvier, B.D., 2012. Immobilization strategies to develop enzymatic biosensors. Biotechnol. Adv. 30, 489–511. https://doi.org/10.1016/j.biotechadv.2011.09.003.

Schmook, F.P., Meingassner, J.G., Billich, A., 2001. Comparison of human skin or epidermis models with human and animal skin in in-vitro percutaneous absorption. Int. J. Pharm. 215, 51–56. https://doi.org/10.1016/S0378-5173(00)00665-7.

Schultz, S.G., Solomon, A.K., 1961. Determination of the effective hydrodynamic radii of small molecules by viscometry. J. Gen. Physiol. 44, 1189–1199. https://doi.org/10.1085/jgp.44.6.1189.

Sheldon, R.A., 2007. Enzyme immobilization: the quest for optimum performance. Adv. Synth. Catal. 349, 1289–1307. https://doi.org/10.1002/adsc.200700082.

Sieg, A., Guy, R.H., Delgado-Charro, M.B., 2004. Noninvasive glucose monitoring by reverse iontophoresis in vivo: application of the internal standard concept. Clin. Chem. 50, 1383–1390. https://doi.org/10.1373/clinchem.2004.032862.

Sieg, A., Guy, R.H., Delgado-Charro, M.B., 2003. Reverse iontophoresis for noninvasive glucose monitoring: the internal standard concept. J. Pharm. Sci. 92, 2295–2302. https://doi.org/10.1002/jps.10492.

Stellwagen, N.C., 1998. Apparent pore size of polyacrylamide gels: Comparison of gels cast and run in Tris-acetate-EDTA and Tris-borate-EDTA buffers. Electrophoresis 19, 1542–1547. https://doi.org/10.1002/elps.1150191004.

Tamada, J.A., Tierney, M.J., Williams, S.C., 2006. Hydrogel Composition for Measuring Glucose Flux. US 7, 150,975 B2.

Tierney, M.J., Jayalakshmi, Y., Parris, N.A., Reidy, M.P., Uhegbu, C., Vijayakumar, P., 1999. Design of a biosensor for continual, transdermal glucose monitoring. Clin. Chem. 45, 1681–1683. https://doi.org/10.1093/clinchem/45.9.1681.

Vasileva, N., Godjevargova, T., 2005. Study of the effect of some organic solvents on the activity and stability of glucose oxidase. Mater. Sci. Eng. C 25, 17–21. https://doi.org/10.1016/j.msec.2004.03.001.

Wang, J., 2008. Electrochemical glucose biosensors. Chem. Rev. 108, 814–825. https://doi.org/10.1021/cr068123a.

Weissberg, H.L., 1963. Effective diffusion coefficient in porous media. J. Appl. Phys. 34, 2636–2639. https://doi.org/10.1063/1.1729783.

Woo, K.M., Chen, V.J., Ma, P.X., 2003. Nano-fibrous scaffolding architecture selectively enhances protein adsorption contributing to cell attachment. J. Biomed. Mater. Res. - Part A 67, 531–537. https://doi.org/10.1002/jbm.a.10098.

Yankov, D., 2004. Diffusion of glucose and maltose in polyacrylamide gel. Enzym. Microb. Technol. 34, 603–610. https://doi.org/10.1016/j.enzmictec.2004.01.008.

Zdarta, J., Meyer, A.S., Jesionowski, T., Pinelo, M., 2018. A general overview of support materials for enzyme immobilization: characteristics, properties, practical utility. Catalysts 8, 92. https://doi.org/10.3390/catal8020092.